JOURNAL OF GEOPHYSICAL RESEARCH: BIOGEOSCIENCES, VOL. 118, 922–939, doi:10.1002/jgrg.20059, 2013

Molecular preservation in halite- and perchlorate-rich hypersaline subsurface deposits in the Salar Grande basin (Atacama Desert, Chile): Implications for the search for molecular biomarkers on Mars

D. C. Fernández-Remolar,[1] G. Chong-Díaz,[2] M. Ruíz-Bermejo,[1] M. Harir,[3] P. Schmitt-Kopplin,[3,4] D. Tziotis,[3] D. Gómez-Ortíz,[5] M. García-Villadangos,[1] M. P. Martín-Redondo,[1] F. Gómez,[1] J. A. Rodríguez-Manfredi,[1] M. Moreno-Paz,[1] G. De Diego-Castilla,[1] A. Echeverría,[6] V. N. Urtuvia,[6] Y. Blanco,[1] L. Rivas,[1] M. R. M. Izawa,[7] N. R. Banerjee,[7] C. Demergasso,[6] and V. Parro[1]

Received 24 September 2012; revised 4 April 2013; accepted 6 April 2013; published 19 June 2013.

[1] Similarities between the Atacama Desert (Chile) and Mars include extreme aridity, highly oxidizing chemistry, and intense ultraviolet radiation that promoted the photochemical production of perchlorates and nitrates. Concentration of these ions under hyperarid conditions led to the formation of nitrate- and perchlorate-bearing deposits in ephemeral lakes, followed by later deposition of chlorides and sulfates. At some locations, such as the Salar Grande, hypersaline deposits have remained unaltered for millions of years. We conducted a drilling campaign in deposits of the Salar to characterize the preservation state of biological molecules. A 5 m deep discontinuous core was recovered and subjected to multitechnique analysis including the antibody microarray-based biosensor LDChip300 and the SOLID (Signs Of Life Detector) instrument, complemented by geophysical, mineralogical, geochemical, and molecular analysis. We identified two units based on the mineralogy: the upper one, from the surface to ~320 cm depth characterized by a predominance of halite and anhydrite, and the lower one, from 320 to 520 cm, with a drop in halite and anhydrite and an enrichment in nitrate and perchlorate. Organic compounds including biomolecules were detected in association with the different depositional and mineralogical units, demonstrating the high capacity for molecular preservation. Hypersaline environments preserve biomolecules over geologically significant timescales; therefore, salt-bearing materials should be high-priority targets for the search for evidence of life on Mars.

Citation: Fernández-Remolar, D. C., et al. (2013), Molecular preservation in halite- and perchlorate-rich hypersaline subsurface deposits in the Salar Grande basin (Atacama Desert, Chile): Implications for the search for molecular biomarkers on Mars, *J. Geophys. Res. Biogeosci.*, *118*, 922–939, doi:10.1002/jgrg.20059.

Additional supporting information may be found in the online version of this article.

[1]Centro de Astrobiología (INTA-CSIC), Torrejón de Ardoz, Spain.
[2]Department of Geological Sciences, Universidad Católica del Norte, Antofagasta, Chile.
[3]Helmholtz Center Munich, German Research Center for Environmental Health, Analytical BioGeoChemistry, Neuherberg, Germany.
[4]Lehrstuhl für Chemische-Technische Analyse und Chemische Lebensmitteltechnologie, Technische Universität Muenchen, Freising-Weihenstephan, Germany.
[5]ESCET, Área de Geología, Universidad Rey Juan Carlos, Móstoles, Spain.
[6]Centro de Biotecnología, Universidad Católica del Norte, Antofagasta, Chile.
[7]Department of Earth Sciences, University of Western Ontario, London, Ontario, Canada.

Corresponding author: D. C. Fernández-Remolar, Centro de Astrobiología (INTA-CSIC), Ctra Ajalvir km. 4, 28850 Torrejón de Ardoz, Madrid, Spain. (fernandezrd@cab.inta-csic.es)

2169-8953/13/10.1002/jgrg.20059

1. Introduction

[2] Various orbital and landed missions indicate that Mars is a planet that has been shaped by volcanic, hydrologic, and atmospheric processes [*King et al.*, 2004; *Murchie et al.*, 2009]. Interactions between igneous activity, the atmosphere, and hydrosphere over the course of Martian geological history are thought to have promoted the production, transport, and precipitation of different soluble anions including chlorides and sulfates [e.g., *King et al.*, 2004]. Salts of these anions have precipitated as cements in aeolian deposits [*McLennan et al.*, 2005] or as sedimentary deposits infilling shallow basins [*Osterloo et al.*, 2008; *Glotch et al.*, 2010]. These deposits were likely formed by supersaturation of solutions produced by leaching of the Martian crust under high evaporative rates, consistent with arid conditions [*Tosca et al.*, 2008]. This is the likely formation scenario of the chloride deposits detected in several outcrops in Meridiani Planum and Terra

Sirenum [*Clark et al*., 2005; *Osterloo et al*., 2008; *Murchie et al*., 2009], which, in some locations, show light-toned materials and polygonal fracturing consistent with the precipitation of salts. More recently, the detection of perchlorates in the soil at the Phoenix landing site [*Hecht et al*., 2009] has provided new insight regarding highly oxidized salts [*Catling et al*., 2010] that, on Earth, are formed in hyperarid desert areas by accumulation of photochemically produced atmospheric compounds in soils where the dissolution rate is very low [*Trumpolt et al*., 2005]. However, they may also be formed by simple precipitation from highly evolved solutions or oxidative weathering based on their close association with nitrates [*Pueyo et al*., 2001; *Jackson et al*., 2006].

[3] Chloride and perchlorate deposits on Mars were likely formed under hyperarid conditions, which have prevented the destruction of sedimentary and paleoenvironmental information [*Lowenstein et al*., 1999; *Hecht et al*., 2009; *Osterloo et al*., 2008]. Chlorides are among the minerals most susceptible to diagenetic alteration due to their high solubility [*Pueyo et al*., 2001]. Therefore, the occurrence of chlorides on Earth and Mars provides evidence of persistent low water activity following salt precipitation. Chloride-bearing salts have a great potential for preservation of biological information for two important reasons: they require water to form, and they provide an excellent matrix for preservation [e.g., *Stan-Lotter et al*., 2006; *Fish et al*., 2002]. Under the conditions of salt precipitation in the Atacama, the biomolecular record of microbial life, which is highly sensitive to hydrolysis and oxidation, has an exceptionally high chance of being preserved with very high fidelity. On Earth, very labile biomolecules, including RNA and DNA [*Eglinton and Logan*, 1991], and long biopolymers have been detected in ancient saline deposits [*Griffith et al*., 2008; *Park et al*., 2009] that are associated to an incipient diagenesis with very low water activity. Although the strong radiation from ultraviolet (UV) light and particle bombardment from solar wind and cosmic rays may make the surface environment of Mars destructive for putative biomolecules, the shallow subsurface is protected, making it a more favorable location to detect signs of life. Therefore, the application of non-oxidative techniques to underground samples is important for the detection of life on Mars [*Navarro-González et al*., 2010], and possible subsurface chloride deposits should be considered high-priority targets in the search for signs of life on the red planet.

[4] In this paper, the astrobiological potential of Martian chloride-rich sedimentary deposits are evaluated based on a multitechnique analysis of analogous ancient chloride-rich and perchlorate- and nitrate-bearing materials formed in the Salar Grande, a hyperarid lacustrine system in the Atacama Desert. This extreme habitat can be considered a Mars analog because of the persistence of hyperarid conditions over millions of years [*Dunai et al*., 2005] and intense UV radiation, which promotes a high rate of oxidant production in the soils and a very low water activity [*Navarro-González et al*., 2003; *Davila et al*., 2008]. To better understand and characterize the preservation potential of the Atacama deposits, we conducted a Mars analog drilling field campaign to search for molecular traces of life in the underground area of the saline deposits, which has been protected from harmful surface conditions [*Parro et al*., 2011b]. Our campaign had two main objectives: (1) to perform mineralogical and geochemical characterization to determine paleoenvironmental changes recorded within the deposits and (2) to evaluate the preservation potential for paleoenvironmental and biomolecular information of this salt-dominated system. Herein we show an extensive geophysical, lithostratigraphic, and mineralogical characterization of the subsurface deposits down to a depth of 520 cm at the drilling. Also, we conduct geochemical and organic analysis at different depths and apply multivariate factor analysis to associate the biomolecular record to the different mineral and lithostratigraphic units.

2. Geology, Sedimentology, and Geobiology of the Salar Grande

[5] The Salar Grande (Figure 1; see supporting information) consists largely of unaltered lacustrine chloride-bearing deposits that were formed in an extensional basin producing a topographically depressed area that promoted subsidence and confined brines [*Reijs and McClay*, 1998]. The formation and growth of the Salar Grande was driven by a regional-scale faulting system (Figures 1 and 2) that formed half-graben systems in two different phases (Oligocene to Early Miocene, and Pleistocene to recent). The half-graben structures produced depocenters for localized sediment trapping during subsidence. Tectonic evolution induced changes in the geochemistry of the saline basins [*Chong-Díaz et al*., 1999; *Sáez et al*., 1999], which started during the Miocene and lasted through the Plio-Pleistocene as an endorheic system fed ephemerally by the Loa River. The hydrological regime of the basin changed drastically after the opening of the Loa drainage to the Pacific Ocean [*Sáez et al*., 1999]. As a consequence, the Salar Grande hydrological system changed from endorheic to exhoreic conditions that were transiently sustained by subsurface inflow. The sedimentary evolution of the Salar Grande basin has been recorded in the form of detrital and chemical sedimentary deposits, which reflect the paleoclimate and tectonic activity in the region. The deposits indicate three different sedimentary episodes [*Chong-Díaz et al*., 1999; *Sáez et al*., 1999]. The first episode began in the Miocene with the deposition of mixed red bed detrital, carbonate, and anhydrite sediments accompanied by lacustrine diatomite materials. Following this sedimentary episode, during the late Miocene, a second sequence of deposition infilled the Salar Grande depression with a detrital unit composed of breccias, gravels, marls, and diatomites grouped as the Quillaua Formation. These deposits were finally capped during the Pliocene to Pleistocene by the massive, predominantly chloride-bearing unit of the Salar Grande named the Soledad Formation, which formed under extreme hyperarid conditions. In this context, such a sedimentary unit can be considered as a lithological and mineralogical analog for the chloride-bearing deposits of Terra Sirenum [*Osterloo et al*., 2008; *Murchie et al*., 2009].

[6] Multiple lines of evidence suggest that diagenesis in the Soledad Formation ceased during the very early stages of the salt precipitation. The exceptional preservation of textures by anhydrite, with no overprinting rehydration phases to destroy the primary sedimentary structures, suggest that in some cases anhydrite was precipitated as a primary mineral under extremely low water activity conditions [*Pueyo et al*., 2001]. Moreover, the presence of nitrates

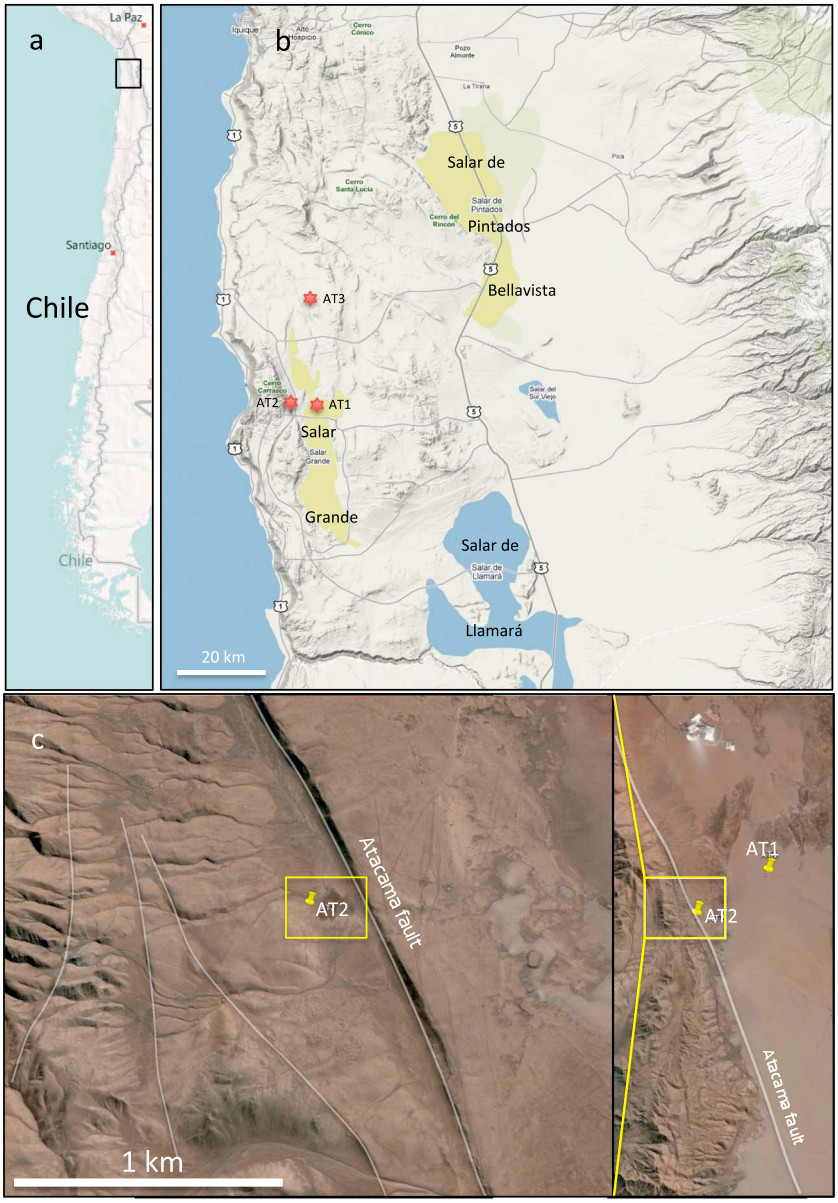

Figure 1. (a) Location of the Salar Grande area (black rectangle) in Chile and (b) the different drilling sites AT1, AT2, and AT3 in the Salar Grande. (c) Satellite image of the Salar Grande margin at the target AT2 showing the main body of salt, Soledad Formation, in AT1. Maps and satellite images copyright 2011 Maplink, Europa Technologies, Google, Inav/Geosistemas SRL and copyright 2011 Cnes Spot Image, DigitalGlobe, Geoeye.

and perchlorates, which are extremely soluble salts, are the result of (1) rapid removal of the water from the system once they formed and (2) persistent very low water activity over the last million years preventing their dissolution.

[7] The geochemistry of the salt formations in modern saline lakes within the Atacama Desert indicate that they are derived from Ca-Cl brines sourced from hydrothermal activity [*Risacher and Fritz*, 2009]. Additional lines of geochemical evidence favor a hydrothermal rather than marine or continental origin for the brines [*Pueyo et al*., 2001]. First, the Soledad halite is depleted in bromide and iodide, consistent with a nonmarine source for the brines [*Parro et al*., 2011b]. Furthermore, analysis of fluid inclusions in the Salar Grande chevron halites have detected Na-K-Cl-SO_4 brines depleted in Mg, saturated in halite and thenardite, and undersaturated in gypsum and anhydrite [*Spiro and Chong Díaz*, 1996]. Isotopic analysis of sulfate $\delta^{34}S$ values in salar salts strongly supports an origin in acidic solutions of a hydrothermal source [*Pueyo et al*., 2001], which could feed the aquifers through the Atacama fault system. Therefore, water inflow and outflow in the Salar Grande, as in many other *salares*, is dominated by fault systems as has been observed in other terrestrial analogs for Mars (e.g., Río Tinto) [*Fernández-Remolar et al*., 2008].

[8] Stable oxygen isotope analysis of Atacama nitrates and perchlorates shows a mass-independent fractionation signature, which most likely reflects formation through atmospheric photochemical reactions [*Michalski et al*., 2004].

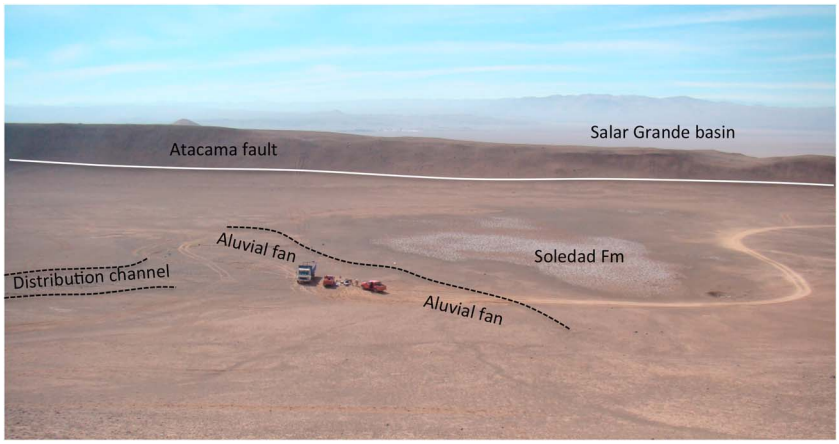

Figure 2. Image showing the geological context for the drilling site at AT2. The vehicles are resting on a distal part of an alluvial fan prograding on the Soledad Formation that corresponds to the white rock. Both sedimentary units are limited to the east by a distinct scarp of the Atacama fault (see Figure 1c).

Stable isotopic measurements for $\delta^{15}N$ and $\delta^{37}Cl$ in nitrates and perchlorates, respectively, also support an origin through long-term atmospheric deposition plus brine concentration occurring under hyperarid conditions [*Chong et al*., 2007; *Catling et al*., 2010].

[9] Microbial and molecular analyses of Atacama salt deposits including soils and old evaporites suggest that they are exceptional materials for long-term preservation. Indeed, the surface of ancient salar salts is a habitat for active photosynthetic communities occupying hydrated microsites in deliquescent minerals including halite [*Davila et al*., 2008; *Wierzchos et al*., 2011]. However, only a few investigations have focused on the microbial analysis of the subsurface Atacama soils. For example, *Lester et al*. [2007] reported on the microbial communities found below the surface to 15 cm. To the best of our knowledge, only one paper has reported an investigation of the microbial and molecular preservation of salt deposits in the subsurface of the Salar Grande. This study by *Gramain et al*. [2011] describes the presence of *Halobacterium* spp., an Archaeal taxon, in 20 m deep cores of the Salar Grande deposits. The application of molecular biology techniques to these samples has revealed the presence of intact DNA, which indicates long-term and high-fidelity biomolecule preservation within salt deposits [*Parro et al*., 2011b].

3. Materials and Methods

3.1. Drilling Procedures

[10] As coolant solutions would contaminate the sample and dissolve the highly soluble salt components, we performed the drilling operations without coolant. However, since chlorides behave in a ductile manner, they have a strong resistance to drilling. As a consequence, several locations were explored to search for a consensus scenario that would satisfy the sampling procedures as well as address the scientific objectives. A detrital deposit of alluvial fan material that graded into the deposits of the basin was determined to be the most feasible scenario satisfying the technical and scientific objectives. One of the locations fulfilling these requirements was found in a marginal depression adjacent to the main salty body of Salar Grande, which is isolated by recent fault activity (Figure 2). It consisted of three different materials: (1) distal deposits of the Soledad Formation composed of detrital sediments cemented by chlorides and sulfates, (2) salty detrital deposits covered by the sulfate-rich crust of panqueque (see auxiliary material), and (3) the prograding lobe of an active alluvial fan. The erosion of volcanic and intrusive materials, with basaltic to andesitic composition, feeds the alluvial deposits dating from the Tertiary [*Chong-Díaz et al*., 1999]. The mixed siliciclastic and salty materials distally grade to an isolated and massive chloride body that provides evidence of ponding and evaporation on top of the massive salts and soils in recent time.

[11] The subsurface samples were obtained by a 5 kW gas Stihl™ power saw modified to accept 85 mm diameter tubing and drill bits that could penetrate to a depth of about 5.2 m. The recovered sample was composed of about 300 cm of core and around 200 cm of fragmented material containing siliceous sands and salt-cemented breccia. Around 1.5 m of continuous core pieces (between 160 and 310 cm depth) was removed and then wrapped in sterile aluminum foil for transport to the laboratory. To decrease friction during drilling, compressed air was injected through the tubing, which ejected the pulverized drill cuttings up and out of the borehole. Samples of this material, ranging from 500 g to 3 kg, were collected with a vacuum sampling system consisting of a commercial aspirator with a new and sterile bag for each sample. Individual samples were labeled and stored for analysis (Table S1). A visual lithological examination in situ of the entire core was performed to build a lithostratigraphical section. All mineralogical, geochemical, and molecular data recovered from the cores were thus characterized in their sedimentary and temporal context.

3.2. Geophysical Survey

[12] Once the drilling target was identified, we completed a resistivity survey to investigate the subsurface distribution of salt deposits below the detrital unit of the fan lobe (Figure 3). Resistivity measurements were made using a Syscal Kid Switch 24 System. This is designed to recover data to 12 m depth, where the length of the sounded profiles was 69 m, at an electrode spacing of 3 m. For interpretation, these data were converted to true resistivity values and

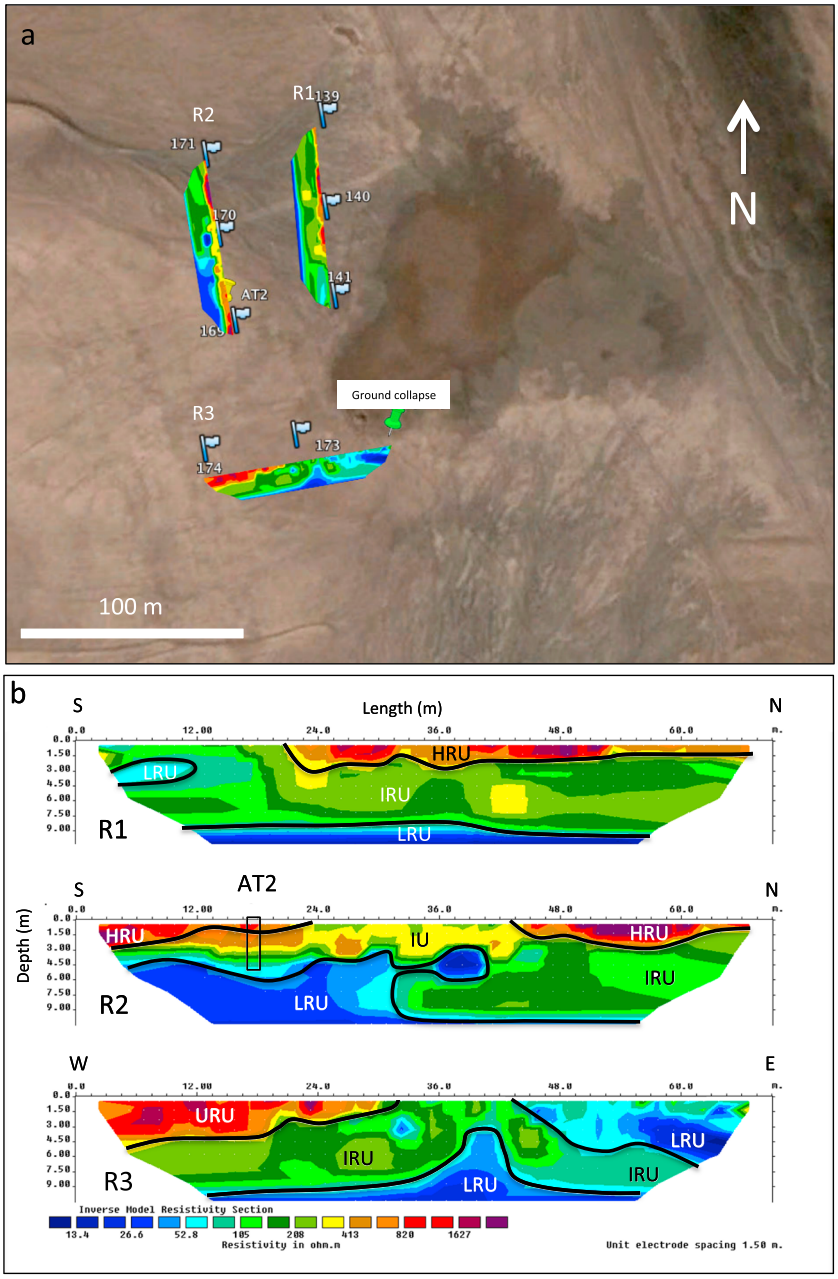

Figure 3. (a) Locations of the three resistivity lines performed for investigating the marginal region of Salar Grande and for location of the optimal drilling target. A 5 m size crater found close to the drilling target is marked as "ground collapse." The three resistivity lines detected (b) three lithological units in base of their electrical properties as a high resistivity unit (HRU), an intermediate resistivity unit (IRU), and a low resistivity unit (LRU) interpreted as upper detrital deposits, dry salts, and wet salts, respectively.

depths through a data inversion procedure. The processing and interpretation of the measured resistivity data were performed using the 2-D finite-difference inversion program of *Loke and Barker* [1996]. The inversion of the data yields a plot that shows a resistivity value for each horizontal and vertical node, which was used to interpret the subsurface. Data processing steps include removing bad data points, selecting the inversion method, and then interpreting the data. Bad data points are determined by computing the root mean square error (RMS) for several measurements in the same quadripole. For each measurement (i.e., each quadripole), several repeated measurements (ranging from 3 to 6) are taken. The data points that exhibit a RMS error lower than 3% are retained, whereas the ones that have higher RMS errors than this are removed from the data set before the inversion procedure.

[13] Three different electrical resistivity tomography (ERT) lines were collected in the area to gain a first-order estimation of the lithological composition in the subsurface. Two ERT lines had a NW-SE orientation, whereas the last one traced an E-W orientation following a perpendicular direction to the two first ERTs (Figure 3). This distribution

was designed to investigate the lateral extent of the lithological units in the subsurface.

3.3. Analytical Methods

3.3.1. Mineralogy and Geochemistry

[14] Samples were observed under a microscope to determine structural, textural, compositional, and microbial information before they were ground for mineralogical and geochemical analyses. For geochemical and mineralogical analysis, they were ground with an agate mortar and pestle to obtain a homogeneous micrometer-sized powder. Mortar and pestle were thoroughly rinsed with water, then distilled water, and finally flamed with ethanol (100% v/v). Mineralogical characterization of samples was performed using a Panalytical X'Pert X-Ray diffractometer operating at 45 kV and 40 mA with copper K-alpha radiation ($\lambda = 1.5414$ Å). The scanning step size was 0.002° per second, covering a 2θ-diffraction angle from 0° to 70°. Geochemical analysis was conducted to obtain the ionic and elemental content of subsurface samples for salts and total rock, respectively. The anionic content and small molecular weight organic acids concentrations were determined by ion chromatography as previously described [*Parro et al*., 2011b]. Whole-rock elemental abundance determination for major and minor/trace elements was performed by using a Panalytical PW2404 X-ray fluorescence instrument bearing a rhodium-anode X-ray tube and coupled to duplex, scintillator, and gas flow detectors. For major elements, samples were prepared as fused beads with lithium tetraborate in a proportion of 0.6 g of sample per fused matrix. For minor and trace elements, samples were prepared as pressed pellets in a mixture with resin, in a proportion of 10 g of sample per 0.6 g of resin (Table S1). Furthermore, anion characterization used the data obtained by *Parro et al*. [2011b]. By using this technique, we obtained a difference between replicate analyses less than 1%.

3.3.2. Molecular Analysis

[15] Molecular in situ determinations were carried out using multiple complementary techniques that have been described in detail for the same field campaign by *Parro et al*. [2011b]. They involve fluorescent antibody microarrays with LDChip300 and SOLID instrument [*Parro et al*., 2008; *Rivas et al*., 2008; *Parro et al*., 2011b] and determination of total protein and sugar content in the field laboratory [*Parro et al*., 2011b].

[16] Crude water-soluble extracts were performed using 30 g of sample as described in *Parro et al*. [2011b]. The final step was dialysis of the extract with a cutoff of 1200 Da. These extracts were used to determine the monosaccharide content by gas chromatography mass spectrometry (GC-MS) as described [*Parro et al*., 2011a].

[17] The LDChip300 contains about 300 antibodies against different molecules including those from cell membranes of archaea and bacteria, extracellular polymers, environmental extracts, proteins, DNA, peptides, exopolysaccharides, amino acids, and others [*Parro et al*., 2011b]. Although the fluorescent intensity as amounts of molecular concentration obtained with the antibody microarray LDChip300 in each antibody-antigen spot is not quantitative, it can be used, however, as a proxy to estimate the molecular diversity and relative biomass distribution. Because all the immunoassays were performed from the same amounts and experimental and scanning conditions, the addition of total fluorescent counts in the positive antigen-antibody reactions was used to estimate the relative biomass between the different sedimentary samples. Additionally, the molecular diversity was obtained through the Simpson Index [*Simpson*, 1949; *Parro et al*., 2011a]

$$S = 1 - \sum_{i=1}^{S} (p_i)^2$$

where S characterizes the molecular diversity in the samples analyzed by the LDChip300; where pi corresponds to the partial diversity computed as a rate between the numbers of counts for each antigen. We used biomass (as total relative fluorescence) and molecular diversity (from antigen data) as the parameters to estimate the molecular preservation over time, similarly as in *Parro et al*. [2011a] for the acidic environment of Rio Tinto. Data analysis of the composition and diversity of samples and antigens promoted the determination of the preservation state of biomolecules and the associated biological information.

[18] Ultrahigh-resolution mass spectrometry was performed with a 12 Tesla SOLARIX Fourier transform ion cyclotron mass spectrometer (FTICR-MS) from Bruker Daltonics, Bremen, Germany, using gentle electrospray ionization in negative ion mode. Extraction of 300 mg of AT2-5e1 sediment sample was done in 1 mL deionized water (1% NH_3 aq). For the analysis of organic compounds, the sample needed to be desalted prior to analysis and the subsequent solid phase extraction (SPE). SPE was made using C18 cartridges (100 mg/1 mL Bakerbond SPE columns, J.T. Baker, Netherlands) following acidification of the sample with formic acid 1% (v/v), which is a well-accepted method in the field of organic geochemistry [*Schmitt-Kopplin et al*., 2012]. Cartridges were conditioned with methanol and acidified water, then the analytes were sorbed on the cartridge. The retained fractions were then eluted with methanol [*Schmitt-Kopplin et al*., 2010] and ready for analysis. The injections were performed using a microliter pump at a liquid flow rate of 120 $\mu L\,h^{-1}$. Nitrogen was used for both sheath gas and curtain gas. A source heater temperature of 200°C was maintained to ensure rapid solvent evaporation in the ionized droplets. Spectra were acquired with a time domain sampling rate of four megawords, and a total of 750 scans were accumulated. Data acquisition and handling were performed using Data Analysis Software from Bruker (Bruker Daltonics, Bremen, Germany). Spectra were externally calibrated on clusters of arginine (10 mg/L in methanol), and accuracy reached values lower 0.1 ppm in day-to-day measurements. Data sets were postcalibrated using ubiquitous fatty acids as internal calibrants.

[19] The lithology, mineralogy, geochemistry, and molecular information were displayed along the lithostratigraphical section that was created during the drilling in order to evaluate their relation to environmental and biological changes over time. Multivariate statistical analysis, filtering, and compilation were carried out using the STATISTICA © StatSoft and PAST programs [*Hammer et al*., 2001].

4. Results

4.1. Local Geological Context and Selection of Sampling Location

[20] The drilling site was selected after exploring several different geological environments in the Salar Grande, including

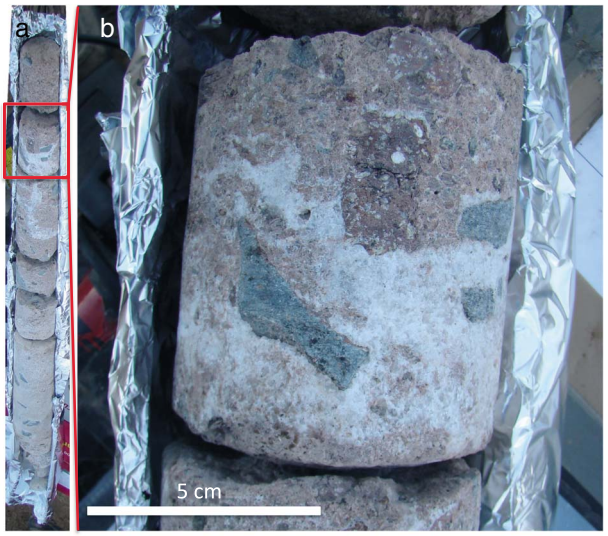

Figure 4. Image of the core at AT2. (a) Full core of 120 cm depth (red box is shown in Figure 4b) and (b) a poorly sorted breccia strongly cemented by halite and other salts crosscut by salt veins.

the Soledad Formation halite-rich deposits, distal lobes of alluvial fans meeting dry gullies, and sulfate-rich soils outside of the Salar Grande rim that are intermixed Soledad Formation and nitrate-bearing deposits (Figure 2). The intermixed Salar Grande rim soils were selected as the best available compromise between the scientific objectives and the technical constraints such as slope and roughness. The target deposits are exposed inside a narrow depression bounded by two subparallel NNW-SSE trending faults. Both structures coalesce to the north as a unique fault closing the depression, whereas, to the south, the fault-bounded valley gradually opens toward the Salar Grande basin. The depression is infilled by active alluvial fans that imbricate and prograde following the structural slope-dipping south (Figure 2) and covering the older lithological units.

[21] Once the general drilling location had been selected, we conducted detailed local mapping over a ~2 km^2 area that included geomorphological, lithological, and molecular characterization, in order to select an optimal sampling location. Several different zones were identified, including the following: (1) wind-blown dust accumulations, (2) salt-enriched mud lobes indicating episodes of recent surface water associated with potential springs, and (3) Soledad Formation deposit (Figure 2) areas showing mineral deliquescence associated with modern microbial activity. Dust accumulation zones were not targeted for drilling due to the likelihood of poor core recovery, whilst zones showing evidence of recent hydrological activity were avoided due to the potential for alteration of the older unit (Figure 2). Following local mapping and detailed investigation of the geological context, we selected one zone as the most feasible to meet both the technical and scientific constraints (Figures 1 and 2). In this zone, the deposits exposed are detrital materials cemented by chlorides and nitrates, which were laterally covered with the Soledad Formation halite deposits and topped by a fine-grained soil and the panqueque gypsum crust. All these sedimentary deposits are covered by thin detrital deposits corresponding to a distal part of an active alluvial fan lobe prograding southward over older deposits (Figure 2).

4.2. Shallow Geophysical Sounding Identified Subsurface Units

[22] Based on geophysical resistivity sounding of the upper ~12 m of sediments, three different subsurface units were distinguished (Figure 3). Resistivity informs about the water content and mineral composition of underground materials, salty or metallic-rich bearing fluids being the most conductive (and less resistive) to the induced electricity current. The shallowest unit (HRU—high resistivity unit—in Figure 3b) consists of 0.5 to 4 m of laterally thinning deposit with an irregular lower boundary and a resistivity above 400–600 Ohm m. It is underlain by a 4–9 m thick intermediate unit (IRU—intermediate resisitivity unit—in Figure 3b) showing resistivity between 75 and 400 Ohm m that has an uneven boundary with the lowest unit. The materials of the lowest unit (LRU—low resistivity unit—in Figure 3b) indicates resistivity below 75 Ohm m, which is the lowest resistivity recorded in the deposits. Resistivity data show significant heterogeneity; however, a general trend of decreasing resistivity from the surface to 12 m depth can be identified (Figure 3). By using the geophysical sounding, the subsurface lithology can be interpreted as upper detrital and dirty salt deposits, dry salts and wet salts, respectively. Indeed, the decrease in resistivity in depth may be the result of a drop in the detrital mineral content or an increase in the water content with increasing depth.

4.3. Lithostratigraphy: Identification of Three Different Sedimentary Units

[23] The petrologic description of core and powder recovered from drilling provided a first-order compositional analysis of the subsurface deposits (Figure 5). Based on structural, textural, and sediment color information, three different lithostratigraphic units were defined. The uppermost ~60 cm consisted of loosely cemented sand with thin laminae of embedded salts, which agrees to then high resistivity unit (Figures 3 and 5). It is followed by ~260 cm of dirty-saline materials (Figures 4 and 5) with textures ranging from heterometric sands to crude conglomerates that are strongly cemented by salts. Boulders and pebbles show angular facets and are covered by thin crusts of whitish-colored salts. The detrital bodies of this unit are commonly crosscut by salt veins ranging from millimeters to centimeters in thickness that connect horizontal salt layers and the salty crusts that coat pebbles (Figure 5a). In some cases, the salt deposits alternate with centimeter-scale beds of less-cemented sandy materials. The intermediate saline deposits overlay ~20 cm of reddish laminated sands, which are followed by more than 2 m of dark red salt-cemented fine sands that alternate with conglomerates. Both halite- and nitrate-rich dry sedimentary deposits are consistent with the intermediate resistivity unit (IRU) (Figures 3 and 5).

4.4. Mineral Composition: High Halite and Anhydrite Content

[24] The X-ray diffraction (XRD) analyses of 10 samples along the stratigraphic section indicate the presence of six different minerals: anhydrite, quartz, albite, diopside, halite,

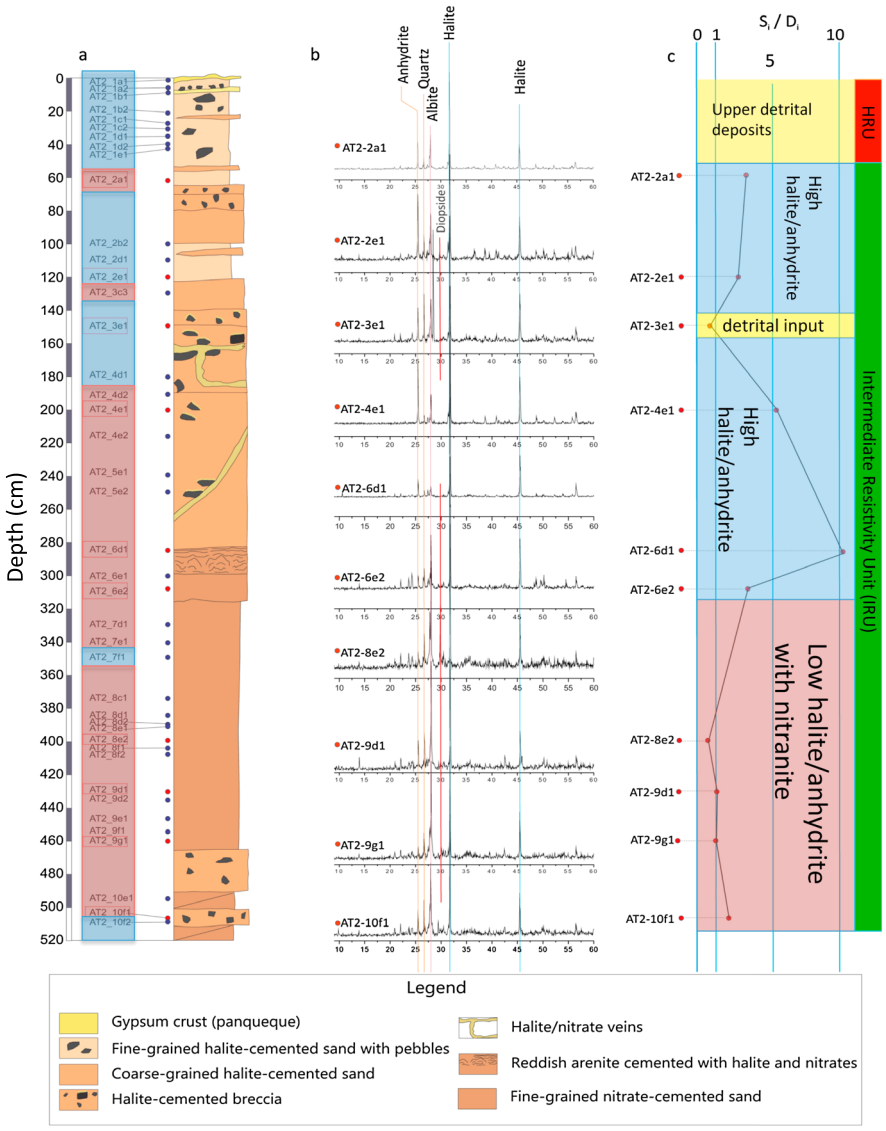

Figure 5. (a) Stratigraphic section and (b) XRD analyses of the materials drilled at AT2. (c) Lithostratigraphic units are characterized by petrological determination and the S_i/D_i index that evaluates the intensity of main XRD peaks in salts (halite plus anhydrite) against detrital minerals (quartz, albite, and diopside). Nitrate-rich unit is characterized by the occurrence of nitranite ($NaNO_3$) by the observation of the reflection at a diffraction angle of 29.5° corresponding to 3.03 Å. Lithostratigraphic units are correlated to the geophysical units, the upper detrital deposits to the high resistivity unit (HRU), and the halite- and nitrate-rich materials to the intermediate resistivity unit (IRU). The low resistivity unit (LRU) would occur at depths below 6–6.5 m with the occurrence of salts containing fluids.

and nitratine (Figure 5b). Although the most abundant mineral species are halite and anhydrite, changes in the relative peak intensities of the various minerals show a trend of decreasing salt content relative to detrital minerals with depth (Figure 5). Two different units can be recognized based on the salt mineral index (SMI), the ratio of the sum of the main (100%) peak intensities above the background of salt minerals (anhydrite and halite) to that of the detrital minerals (quartz, albite, and diopside) (Figures 5c and S1). The intermediate unit, from ~60 cm to ~320 cm depth, is characterized by a SMI > 1, with a predominance of halite and anhydrite. The lower part of this unit has a lower concentration of siliciclastic minerals with a few minor siliciclastic-rich beds (e.g., at 160 cm depth) reflecting a high detrital input. Below 320 cm depth, the sum of XRD peak intensity in the detrital minerals equals the chemical precipitates (SMI ~ 1) likely as a response to an increase in the siliciclastic supply to the sediments, salt removal, and/or poor preservation of salts.

[25] Nitratine ($NaNO_3$) was detected (Figures 5b and S1–S5) below 320 cm by XRD in samples AT2-9g1, AT2-10f1, and AT2-9d1 and possibly AT2-6e2 (Figure S2) near the base of the overlying unit. Identification of nitranite was based on the observation of a reflection at a diffraction angle of 29.5°

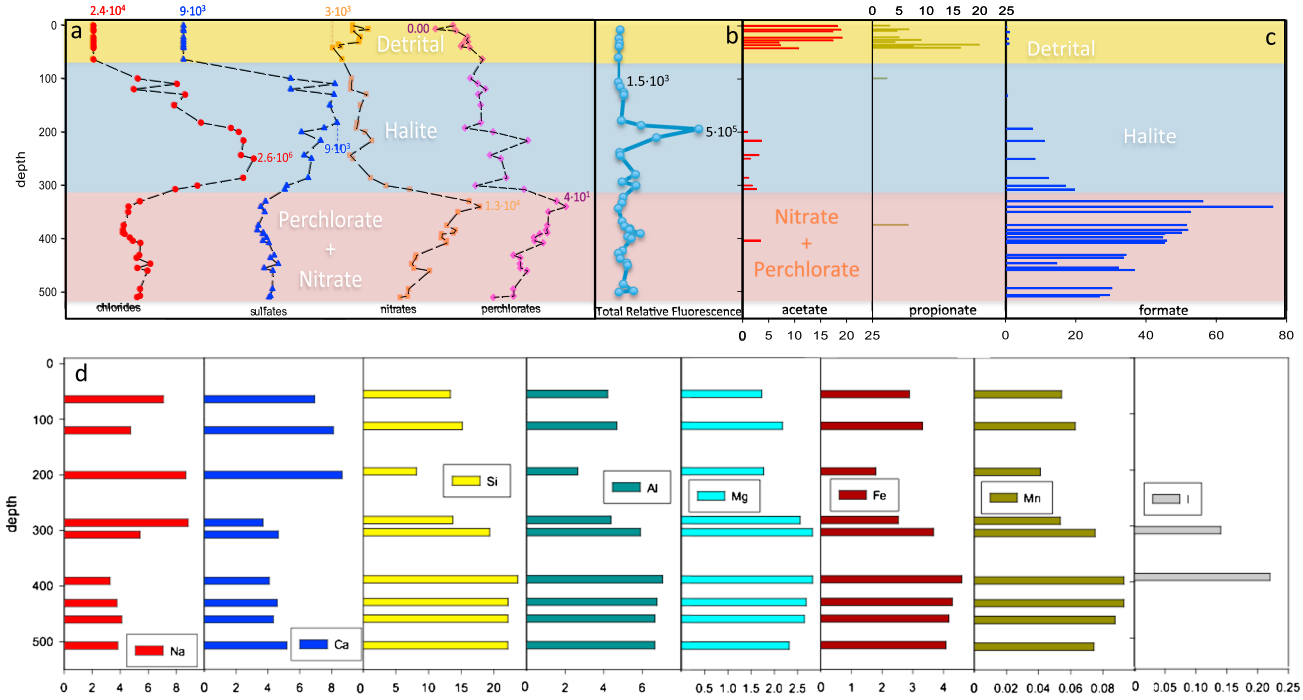

Figure 6. Geochemical scatterplot and bar diagrams of borehole AT2 (depth in cm) including inorganic and organic composition in parts per million, as well as molecular detection (total relative fluorescence). (a) Shading indicates the distribution of the chloride (gray) and perchlorate and nitrate-rich (light orange) in parts per billion units. The upper scatterplot projects anions as sulfate (SO_4^{2-}), chloride (Cl^-), nitrate (NO_3^-), and perchlorate (ClO_4^-) against borehole depth, showing an increase in nitrate$^-$ and perchlorate, whereas sulfate and chloride concentrations decrease below 320 cm depth. (b) Total relative fluorescence (TRF) units obtained with different antibodies after LDChip300 immunoassay that is consistent with the presence of the three lithological units. (c) Concentration of small-sized organics such as acetate, propionate, oxalate, and formate along the depth in the borehole AT2 and in relation to the three different stratigraphic bodies; concentration units are in micrograms per gram of sample. (d) Bar diagrams for elemental geochemistry of the subsurface samples (wt %) also shows a change in the concentration according to the increment observed for perchlorate and nitrate in the same way for the iodine that corresponds to salts formed under a very low water activity. The presence of a high concentration in nitrate and perchlorate suggests that the lower unit is a nitrate/perchlorate-bearing sediment formed under much harsher conditions of saturation than the halite sediments.

corresponding to 3.03 Å, consistent with the (10–14) reflection of nitranite.

4.5. Subsurface Geochemistry

[26] Elemental and ionic geochemical characterization of subsurface samples recovered from site AT2 (Figure 6) is in agreement with the mineralogy determined by XRD analyses. The two different sedimentary units defined using the SMI above can also be identified geochemically. The upper unit is characterized from the surface to ~60 cm with a low concentration in chloride and sulfates. The intermediate unit (from ~60 cm to ~320 cm) has a high concentration of chloride and sulfates. Below 320 cm to at least 520 cm depth, the lower unit shows a strong increase in the concentration of perchlorate and nitrate anions with a decrease in the total concentration of chloride plus sulfate anions (Figure 6a). Moreover, element concentration values provide complementary data to trace both sedimentary deposits in the shallow subsurface. Elements hosted primarily in detrital minerals (Si, Al, Mg, Fe, and Mn) plot complementary to the chloride and sulfate data. Sodium and calcium found predominantly in halite and anhydrite show the same trend as observed for both minerals and the chloride and sulfate anions (Figures 5, 6, and S1). Additional highly soluble anions including iodine were detected in samples of the perchlorate- and nitrate-rich lower unit, supporting supersaturation of the brines (Table S1).

4.6. Distribution of Organic Composition and Patterned Small Organic Acids

[27] We performed two independent organic analyses, including ion chromatography (IC) and FTICR-MS, of several samples from the borehole, which both yield positive results. IC detected four low-mass organic compounds: acetate, propionate, formate, and oxalate (Figure 6c). Acetate and propionate have very similar distributions, showing the highest concentrations (up to ~20 ppm) in the first 50 cm of the section, with much lower concentrations and a more sparse distribution below. Formate occurs sparsely along the first 200 cm of section, with very low concentrations

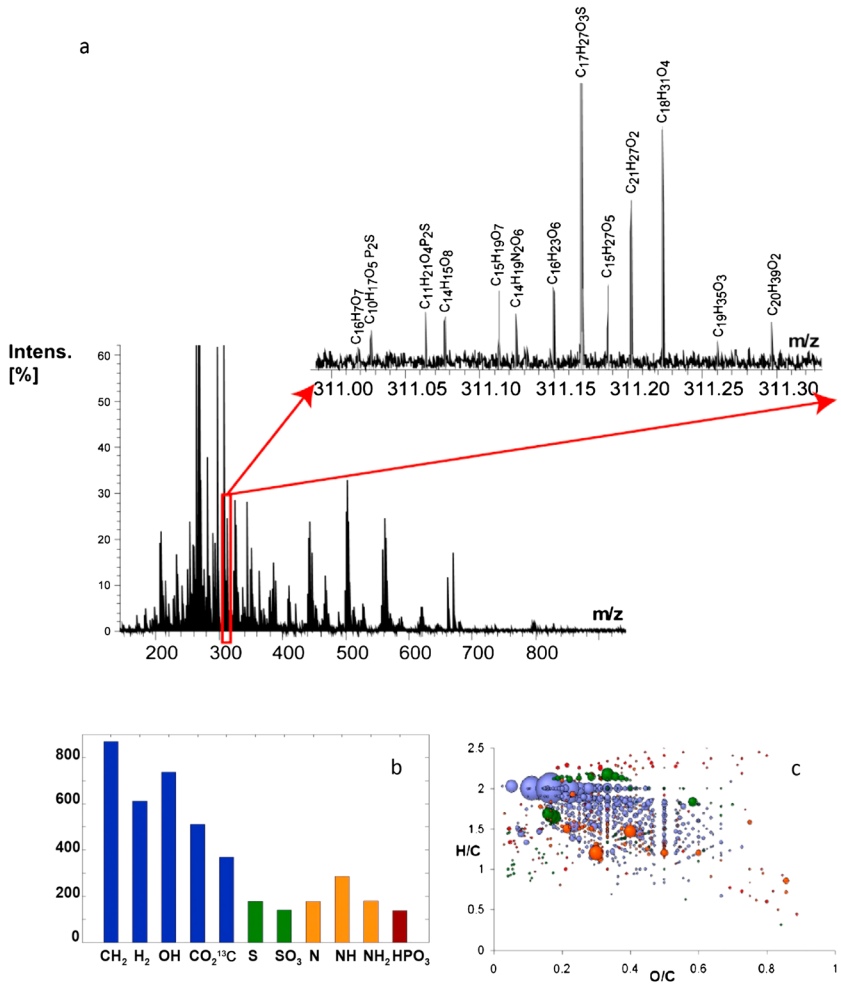

Figure 7. (a) ESI(−)-FTICR mass spectra (150–1000 Da) of AT2-4e1 (C18-SPE extracted sediment from Atacama Desert). The insert figure shows an extended mass range m/z 311.00–311.30 (0.3 Da) in which plausible molecular formulas are given on the basis of their high mass accuracy (lower 0.5 ppm) and mass resolution (R = 800.000 at m/z 311). (b) frequency histogram of the exact mass differences corresponding to CH_2,H_2, OH, CO_2, ^{13}C, S, SO_3, N, NH, NH_2, and HPO_3 (error range 0.1 ppm). (c) H/C versus O/C van Krevelen diagram (dots: blue, CHO; green, CHOS; orange, CHON; red, CHONS). Both Figures 7b and 7c show the consistency in homologous structural series in CHO compounds.

(few ppm) in the uppermost 50 cm, increasing to an average of 15 ppm from 200 to 300 cm, and is much more abundant (up to ~75 ppm) in the nitrate- and perchlorate-rich unit below ~300 cm depth.

[28] The high concentration and diversity of molecular biomarkers detected by the immunosensor LDChip300 led to the selection of sample AT2-4e1 for ultrahigh-resolution mass spectrometry. The spectrum of the water extract of sample AT2-4e1 provided several thousand signals in the mass range 150–1000 Da (Figure 7a). These were assigned to their corresponding molecular compositions and classified as CHO, CHOS, CHON, CHONS, CHOP, CHNP, and CHONPS. The frequency in the presence of exact mass differences corresponding to CH_2, H_2, OH, CO, SO_3, NH, NH_2, and HPO_3 is shown in Figure 7b. The van Krevelen diagram (Figure 7c) illustrates a projection of the relationship between the atomic ratios O/C (*x* axis) versus H/C (*y* axis) of each assigned molecule in the experimental spectrum. All analyzed molecules have an m/z from 150 to 350 Da with a H/C ratio greater than 1 and an O/C ratio less than 1.

4.7. Biochemical Analysis Through the Stratigraphic Units

4.7.1. Sugar Content and Its Distribution With Depth

[29] We determined the monosaccharide composition in the polymeric crude extracts of several samples at different depths (Figures 8 and S6–S8). We detected several monosaccharides such as glucose, galactose, mannose, xylose, or glucuronic acid that usually are structural components of microbial extracellular and cell wall polysaccharides [*Fazio et al.*, 1982]. Other monosaccharides such as inositol and mannose may come from the intracellular compatible solute pool (e.g., di-myo-inositol-1,1′-phosphate, mannosylglycerate, or di-mannosyl-di-myo-inositol-1,1′-phosphate) used by microorganisms to cope with saline environments [*Santos and da Costa*, 2002]. These results indicate the potential for

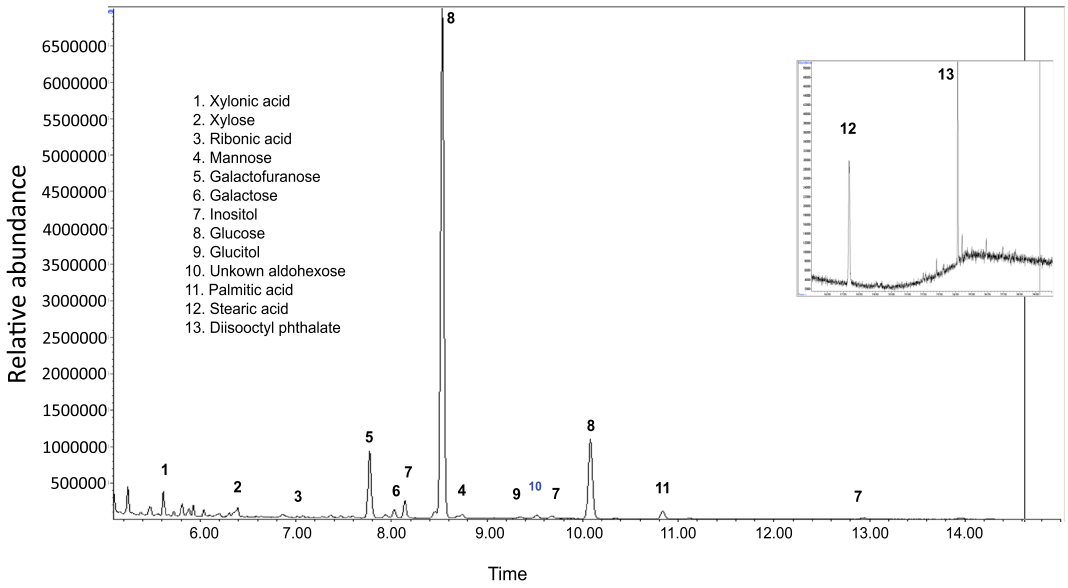

Figure 8. Monosaccharide content in sample AT2-4e1 from 2 m depth. GC chromatogram showing the most abundant monosaccharides in crude extracts from sample AT2-4e1 as identified by GC-MS analysis. The names of the sugars corresponding to the different peaks are indicated. The insert shows other compounds detected at longer retention times.

a higher degree of preservation of the biological polymers in all the stratigraphic units identified.

4.7.2. Distribution of the Biomolecules Detected With LDChip300

[30] We performed the molecular analysis of the subsurface samples with the immunosensor LDChip300 in SOLID3 instrument and in the field laboratory [*Parro et al*., 2011a, 2011b]. If the target molecule (antigen) was present in the aqueous extract of the sample, a fluorescent signal was produced and quantified, enabling the generation of an immunogram from each sampled stratigraphic level (Figures S9–S11). Although most of the collected samples produced positive results, the signal and diversity of molecules detected were especially high at a depth of ~2 m in samples AT2-4c1, AT2-4e1, and AT2-4e2 (for a complete list of antigens and antibodies, see *Parro et al*. [2011b]) (Figures S10 and S11). The total relative fluorescence was obtained by adding the signal of the positive antigen-antibody reactions for each sample after LDChip300 immunoassay. The total relative fluorescence (TRF) for each antigen-antibody spot was determined as reported [*Parro et al*., 2011b]; briefly, the TRF for each antibody spot was calculated using the following equation: $TRF = (F_{sample} - F_{blank} - 3Fav_{control\ spots})$, where F_{sample} is the fluorescent intensity of the analyzed sample at 635 nm minus the local background as quantified by the GenePix Pro software, F_{blank} is the fluorescence intensity of the blank (negative control) sample, and $Fav_{control\ spots}$ is the average fluorescent signal of the control spots. Said control spots were those containing only bovine serum albumin (BSA), buffer, and others corresponding to the pre-immune antisera (more than 50). We always subtract 2–3 times the $Fav_{control\ spots}$ as a stringency cutoff to minimize false positives.

[31] A scatterplot of total fluorescence suggested the occurrence of distinct layers within the stratigraphic column that showed signals in total fluorescence (Figures 6b and S9), but that the background levels between these signals dropped back down to the same levels as at the surface. There are specific horizons within the layers that have higher concentrations of biomolecules that would suggest that those specific horizons show a smaller target with greater likelihood of finding biosignatures, something that would be invaluable in searching for life on Mars. Such specific horizons are arranged in three subsurface zones with depth (Figures 6b and S9): an upper area with levels showing very low signal (average of $1.9 \cdot 10^3$ relative fluorescence units—rfu) associated to detrital sediments, an intermediate zone with most of levels with signals above $20 \cdot 10^3$ rfu (average of $59.1 \cdot 10^3$) in the chloride-rich deposits, and a lower area with a high average signal ($39 \cdot 10^3$ rfu), which corresponds to the nitrate- and perchlorate-rich sediments. Such distribution suggests the presence of biomolecules at relatively high concentrations in levels enriched in salts below 60 cm, with a maximum in the intermediate area, which corresponds to the halite-rich deposits. The total fluorescence signal as a function of depth shows two local maxima, one at 200 cm and another one at 398 cm depth (samples AT2-4e1 and AT2-8e2, respectively), which also meet a maximum in the concentration of chlorine (Figure 6a).

[32] Multivariate factor analysis of the LDChip300 data for each sampled location, with antibodies clustered according to frequency of occurrence, shows that the detected molecules cluster in three groups (Figures S12 and S13): (1) very common antibodies (Figure 9), here referred to as major antibodies (MA), which mostly occur in the salt-rich area below 60 cm; (2) antibodies occurring in three to five samples, which show a preferential distribution to the saltier areas but also show some bimodal distribution in both stratigraphic groups; and (3) antibodies occurring in one or two samples, which are more common in the halite-rich lower unit. The MA distribution along the 520 cm section indicates the presence of preserved biomolecules, with local maxima at depths of 200 and 405 cm, which correspond to the chloride- and perchlorate-

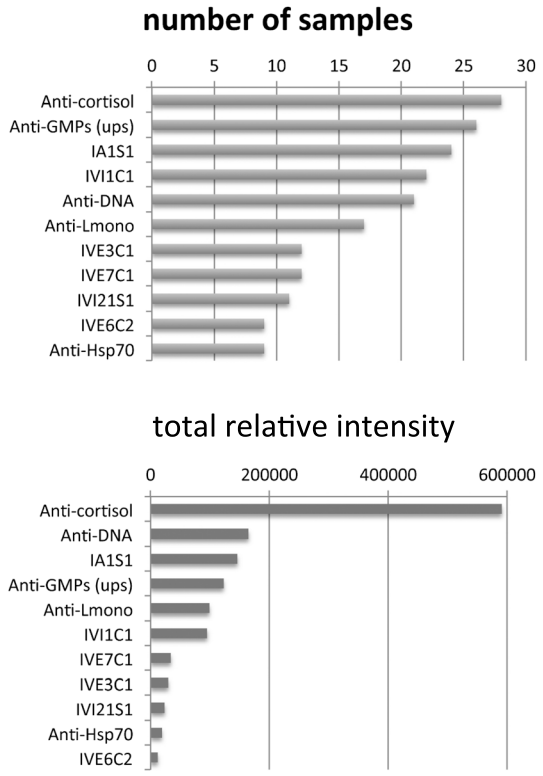

Figure 9. Bar diagrams showing the occurrence of the major positive antibodies per sample and abundance based on the sum of total fluorescence intensity from LDChip300 results.

rich units, respectively (Figures 6b, 9, and S9–S11). The MA results show that different groups of microbial life were present at the time of deposition of the salty materials of the Salar Grande. Interestingly, the highest signal for the MA is obtained with the anti-cortisol antibody (Figures 9 and S10), which suggests the presence of a high input of steroid-like biomolecules in the saline deposits, possibly including eukaryotic steroids such as ergosterol (produced by fungi), or cyclic triterpenes (e.g., hopanols) and other cyclic by-products (e.g., polycyclic aromatic compounds) from bacteria. A record of biomolecules is also represented by positive results for nucleic acid derivatives, including two anti-cGMP antibodies and one anti-DNA antibody, which is characteristic of well-preserved biological polymers. The pattern obtained with these anti-nucleic acids antibodies along the borehole is similar to that of anti-cortisol, which is consistent with the presence of eukaryotes (e.g., fungi) as well as prokaryotes (bacteria and archaea). Positive results for antibodies IA1S1, IVI1C1, IVE3C1, and IVE6C2 suggested the presence of microbes belonging to different groups of Proteobacteria (Table 1; *Parro et al*. [2011b]) that include several forms of acidophiles. Interestingly, antibodies IVE7C1 and IVI21S1, from the halophiles *Halothiobacillus neapolitanus* and *Salinibacter rubber*, respectively, gave peaks with a high intensity at a depth of around 200 cm in the chloride-rich unit and also some minor peaks at various depths in the perchlorate-rich unit below 320 cm.

[33] The plot of the Simpson Index molecular diversity against the total relative fluorescence (as shown in *Parro et al*. [2011b]) for each sample of AT2 shows a specific distribution regarding preservation of biomolecules (Figure 10a). Herein, the Simpson Index evaluates the preservation potential for each level on the basis of the molecular concentration and diversity, in the same way that it has been designed to determine the biological diversity in the ecosystems [*Simpson*, 1949]. Samples are clearly arranged in three different areas: (1) high Simpson Index (>0.90) and total relative fluorescence (TRF) including samples AT2-4d2, AT2-4e1, and AT2-4e2; (2) high to low Simpson Index (0.40 to 0.90) and low TRF ($<8 \cdot 10^4$); and (3) very low Simpson Index (<0.40) with TRF $<8 \cdot 10^4$. We have performed similar data analysis for antigens with a Simpson Index >0.6 that have included the number of occurrences of each antibody for a better classification of data (Figure 10b). As a result, antibodies anti-cortisol, anti-GMP(bio), anti-GMP(ups), anti-dsDNA(hu), anti-dinitrophenol, IA1S1, and IVI1C1 showed the highest record for the three parameters as the Simpson Index, the occurrence number, and the total relative intensity. Proteinaceous compounds detected with anti-Hsp70, anti-ModA2, anti-DhnA0, and anti-ASF1, together with antibodies targeting more specific microbes (e.g., IVE6C2 and IVI9C1), are ranked immediately below with a Simpson Index <0.9, an occurrence number lower than 15, and a TRF under $2 \cdot 10^5$. The data analysis performed for each antibody suggested a similar distribution based on abundance and persistence of biomolecules in the analyzed samples (Figure 10b). Plotting the TRF and the Simpson Index (>0.6) against the occurrence number in AT2 samples, the antibodies were sorted out in

Table 1. Description of the Major Antibodies (MA) as the Most Relevant Showing Positive Reaction With Samples From Borehole AT2 and the Biological Information Obtained When Detected in the Subsurface Samples

Major Antibody	Target antigen or Immunogen	Biological Information in Sample
Anti-cGMP(ups)	Cyclic GMP-BSA	Nucleic acid derivatives from bacteria
Anti-cortisol	Cortisol 21-hemisucc-thyroglobulin	Steroid-like lipids in bacteria and eukarya Triterpene-like molecules
IA1S1	Extracellular material from Río Tinto water rich in Gammaproteobacteria	Gammaproteobacteria
IVI1C1	*Pseudomonas putida*	Gammaproteobacteria
Anti-DNA	Double-stranded DNA	Presence of DNA
Anti-*Lmono*	*Listeria monocytogenes*	Lipoteichoic acids from Gram-positive bacilli
IVE3C1	*Acidithiobacillus ferrooxidans*	Gammaproteobacteria
IVI21S1	*Salinibacter ruber*	Halobacteriaceae (halophilic bacteria)
IVE6C2	*Acidithiobacillus caldus*	Gammaproteobacteria
IVE7C1	*Halothiobacillus neapolitanus*	Halophile bacteria
Anti-Hsp70	Hsp70 (DnaK) protein (*Mycobacterium tuberculosis*)	Heat shock and salt stress protein

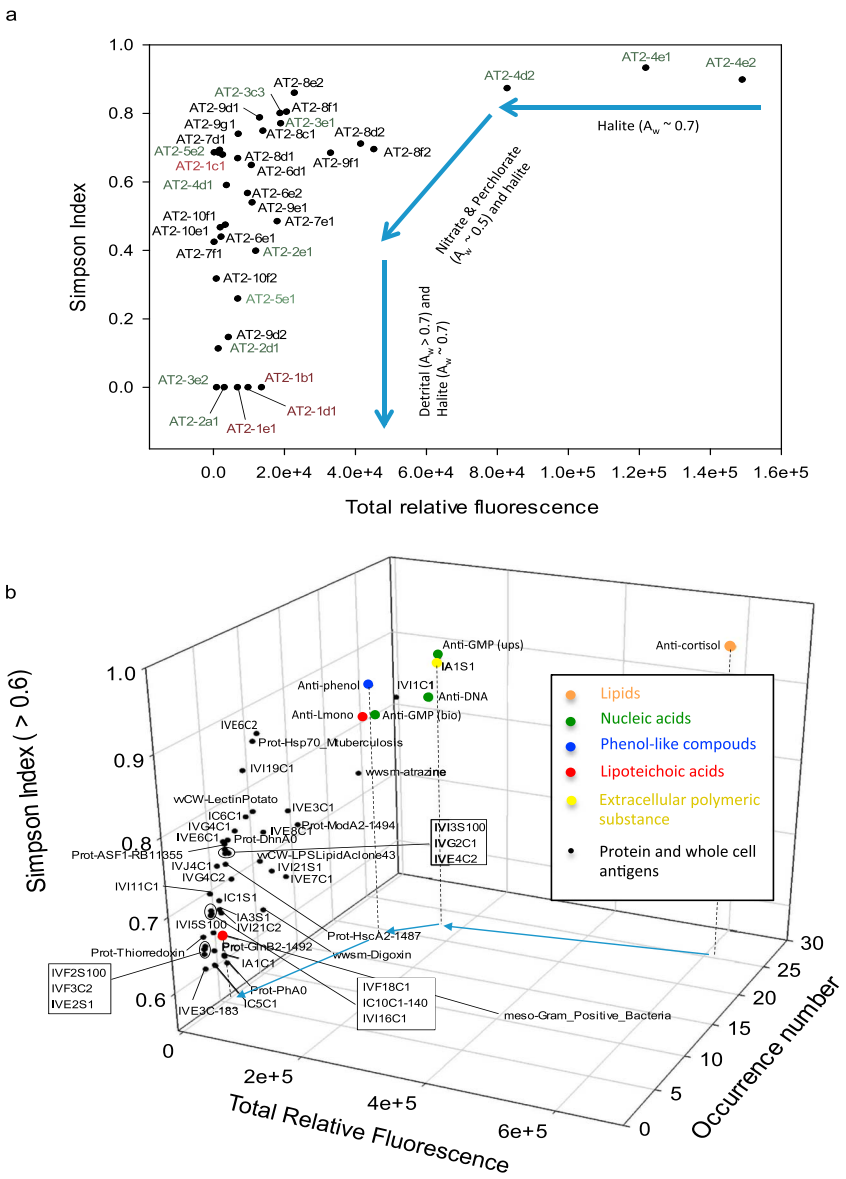

Figure 10. (a) Scatterplot showing the total relative fluorescence and Simpson Index in samples recovered at AT2. Sample distribution suggests that they are arranged based on their mineral and geochemical composition where arrows are pointing to the geochemical trends in preservation regarding the water activity (A_w), which go from high preservation in halite to low preservation potential in detrital deposits. (b) Three-axed plot showing the total relative fluorescence, Simpson Index, and the occurrence number of antigens having a Simpson Index >0.6. The presence of antigens such as anti-cortisol (likely lipids and triterpene-like compounds) and anti-dinitrophenol scored high in the three parameters, suggesting a high persistence over time. However, the detection of nucleic acids (anti-DNA(hu)), proteins (e.g., anti-ModA2, anti-DhnA0, anti-ASF), and lipoteichoic acids (anti-Gram-positive bacteria and anti-Lmono) also showing high record in the three parameters support a high preservation potential for the chloride and nitrate/perchlorate-rich deposits. Blue arrows are showing changes in the three parameters (persistence) for each antigen.

four different groups (Figure 10b): (1) antibodies grouped with an occurrence number higher than 25 and both high TRF ($>4 \cdot 10^5$) and Simpson Index (>0.9) including the anti-cortisol; (2) antibodies grouped with an occurrence number of ~25, a TRF of ~$1 \cdot 10^5$ to $4 \cdot 10^5$, and a Simpson Index of 0.85–0.9, such as anti-dsDNA(hu), anti-cGMP(bio), anti-GMP(ups), anti-dinitrophenol, IA1S1, and IVI1C1; (3) antibodies grouped by a Simpson Index ranging between 0.6 and 0.8, a TRF of ~10^5, and an occurrence number lower than 20 (e.g., anti-Gram-positive, anti-Hsp70, anti-ModA2, anti-DhnA0); and (4) antibodies grouping with a Simpson Index lower than 0.6, low TRF ($<5 \cdot 10^4$), and an occurrence lower than 5. As a main result, Figure 10b approaches labile with resistant biomolecules regarding to degradation degree (e.g., nucleic acids versus steroid-like compounds), which currently occurs in recent materials or sediments with a very high preservation potential. This suggests that both the chloride and nitrate-rich deposits have a high preservation potential.

5. Discussion

[34] A multitechnique approach to the sample analyses of salty materials at site AT2 in the Salar Grande revealed that the two different saline units, chloride-rich and perchlorate-rich (Figures 4 and 5), have preserved diverse molecular and structural evidences of ancient microbial activity. The subsurface distribution of nitratine detected by XRD (Figures 5b and S2–S5) is consistent with geochemical data showing elevated nitrate (and perchlorate) in the same samples. First, the results indicate that there are specific distributions of small organic acids such as formate in both units (although at much higher concentration in the perchlorate unit). This peculiar distribution is complementary to the occurrence of acetate and propionate whose appearances are limited to the upper detrital unit enriched in chloride. Additionally, although scarce, oxalate has a higher concentration in the chloride-rich unit. Assuming that acetate, propionate, oxalate, and formate are molecules involved in different metabolic processes in microbes [*Dutton and Evans*, 1996; *Chin and Janssen*, 2002], such a distribution along the section could suggest distinctive metabolic pathways operating on the surface versus the subsurface. Formate is one of the products released by fermentation under strong anaerobic conditions when catabolizing glucose as a substrate, which has been detected along the section (Figures 8 and S6–S8). Formate thus produced may have been incorporated into the chlorides, nitrates, and perchlorates during the burial of microbes under low water activity. Once the salt minerals precipitated, strong anaerobic conditions were favored inside porosity voids, which promoted the complete removal of oxygen by microbial activity. In this scenario, formate accumulation resulted from the closing of the system to exchange with the atmosphere by salt precipitation. It is also possible that the strong signal of formate in the nitrate- and perchlorate-rich unit could have been the result of the partial oxidation of organic compounds when exposed to perchlorate solutions [*Navarro-González et al*., 2010] or through unknown metabolic pathways using organic compounds as electron donors. Therefore, both microbial metabolism and abiotic partial oxidation may have combined to induce the enrichment in formate in the nitrate- and perchlorate-rich unit, whereas in the chloride-rich unit, microbial fermentation under anaerobic conditions could be the main process to produce formate at a lower concentration. Very recently, *Blanco et al*. [2012] have reported the presence of benzenehexacarboxylic acid (mellitic acid) at the parts per billion level in these samples by means of a specially designed inhibitory immunoassay. The mellitic acid distribution pattern was similar to the acetic and propionic acid ones, that is, preferably in the upper parts of the drill. Such a pattern indicates that these carboxylic acids may originate from the photo-oxidation of different complex organics (e.g., black carbon) and heterogeneous biological material from the surface.

[35] The detection of organic compounds and biomolecules by mass spectrometric techniques provides strong support for organic preservation under the hypersaline conditions of the Atacama deposits. Analysis of sample AT2-4e1 provided evidence of preservation of diverse organic molecules ranging in mass up to more than 700 Da (Figures 7a and 7b). The organics detected show rather similar structural characteristics, with high aliphaticity and low oxygen content (no aromatic compounds, typical of higher organisms such as plants, were observed, consistent with a microbial origin for the organic compounds). It has been reported that high H/C ratios result from high concentrations of aliphatic compounds, reflecting the preservation of microbial biomolecules [*Schmidt et al*., 2009]. The decrease in the O/C ratio could be due to the transformation of oxygen-rich molecules via a selective biodegradation process [*Kim et al*., 2006]. A lower content in oxygen-rich organic molecules and the presence of long-chain C-bearing compounds also suggests a low degradation stage for part of the organic input in the ancient chloride-rich sediments. The detection by mass spectrometry of NH_2 and HPO_3 fragments, which are common constituents of amino acids and nucleotides, also suggests high-fidelity preservation of organics in the saline samples recovered at AT2 in the subsurface (Figure 7b).

[36] The positive microarray immunoassay in the subsurface samples recovered at AT2 suggests a high preservation potential for the biological information recorded in the saline deposits. The high-intensity signal of the anti-cortisol antibody (Figures 9 and S10) indicates the presence of steroid-like lipids (among the most degradation-resistant biomolecules) (Table 1; *Parro et al*. [2011b]). On the other hand, the antibodies for molecules that are more abundant and extend over all living forms as DNA and other molecules such as cGMP (Table 1) show a high intensity relative to that observed for antibodies such as IVE3C1, IVE7C1, or anti-Hsp70 designed for specific bacterial strains or proteins (Table 1 and Figure S11). Antibodies including IVI1C1 and anti-Lmono (recognizing lipoteichoic acids), which bind to molecular structures in the cell wall and are common to large bacterial groups such as Proteobacteria and Gram-positive Firmicutes [*Parro et al*., 2011b], also show intensities higher than the antibodies detecting proteins.

[37] Precipitation of halite and perchlorate-bearing salts occurs under low water activity conditions. Halite precipitates at a water activity of around 0.75, whereas perchlorate minerals are formed at a much lower water activity of about 0.5 [*Houtkooper and Schulze-Makuch*, 2010]. Despite the low water activity for perchlorate formation and highly oxidizing nature of perchlorate-rich solutions, a record of ancient microbial communities are preserved in these rocks in the form of diverse well-preserved biomolecules (Figures S10 and S11). The water activity of brines that produced sulfates and iron oxides on Mars has been estimated at ~0.3–0.5 [*Tosca et al*., 2008]. Given that perchlorate-rich solutions, such as those investigated here, can preserve biological information under low water activity and highly oxidizing conditions, it is reasonable that similar deposits on Mars may also have a high preservation potential and may have recorded evidence of putative biomolecules. Although microbial metabolic activity might not be feasible under the current highly oxidizing and extremely low water activity conditions on Mars, the preservation of biomolecules by putative past microbial life may be possible and even favorable under the conditions similar to those during the emplacement of the units studied here.

[38] Although the monosaccharide pattern was similar along the different depths analyzed (Figures S6–S8), plotting the Simpson Index against the TRF of each sample immunoassay (Figure 10a) [*Parro et al*., 2011b] showed, however, an arrangement of samples in three different groups on the basis of their composition and stratigraphic distribution (see section

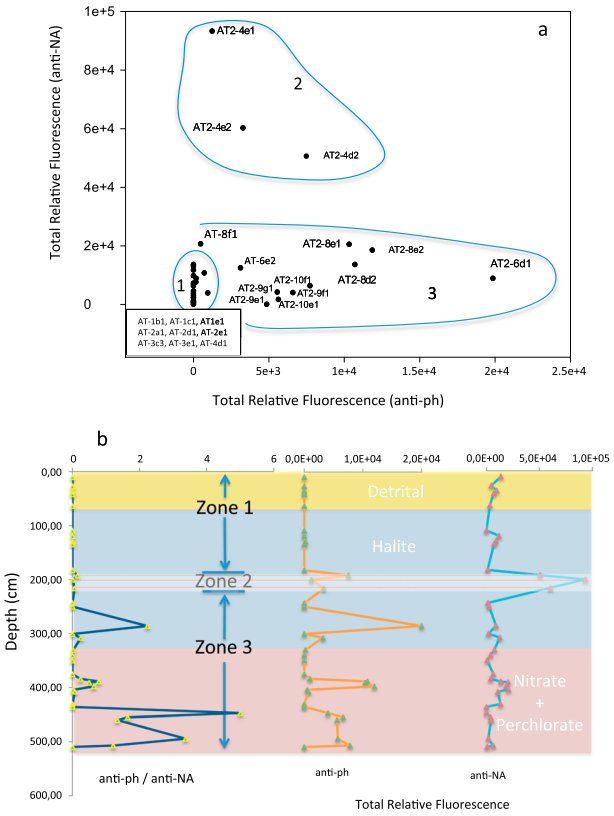

Figure 11. (a) Scatterplot showing the total relative fluorescence of anti-dinitrophenol (anti-ph) against the sum of the total relative fluorescence of nucleic acids (anti-DNA(hu), anti-GMP(ups) and anti-cGMP(bio)). The plots arrange samples in three different trends that agree with the lithological composition and stratigraphic position. (b) Stratigraphic variation of rating the total relative fluorescence of anti-dinitrophenol (anti-ph) against the sum of the total relative fluorescence of nucleic acids (NA) (anti-DNA(hu), anti-GMP(ups), and anti-cGMP(bio)); stratigraphic variation of the total relative fluorescence of anti-dinitrophenol (anti-ph) and the sum of the total relative fluorescence of nucleic acids (anti-NA) have been also included for comparison. As a result, three different zones (1 to 3) in the lithostratigraphic section can be recognized on the basis of preservation.

4.7.2). Such sample arrangement suggested the emergence of a preservation gradient for biomolecules depending on the physical and chemical conditions but not the age of the samples. In fact, older samples that belong to the nitrate- and perchlorate-rich and the chloride-rich units have a higher record in the Simpson Index and the TRF. Although they show a high content in preserved biomolecules, such samples were mainly formed under a water activity below 0.7 and high UV radiation that could potentially limit the development of microbial communities. Under these circumstances, the release of biomolecules to the sediments would decrease but, paradoxically, experience a high increase that can be associated to the preservation potential of salts. On the other hand, those samples obtained in the upper detrital material that were likely formed in less saline solutions ($W_a > 0.7$) show a much lower TRF and a lower record for the Simpson Index that suggests a lower degree for the preservation of the molecular record. It goes against the idea of the high production of biomolecules by a more abundant and diverse community exposed to conditions of lower salinity and stress [*Navarro-González et al.*, 2003]. On the other hand, this could be a consequence of a higher exposure of biomolecules to surface oxidant-rich solutions in the environments that currently produce detrital deposits.

[39] The distribution of positive antigen-antibody reactions in Figure 10 showed that molecules with a higher resistance to degradation or were the product of degradation (e.g., anti-cortisol and anti-dinitrophenol) paradoxically occurred together with the most labile biomolecular compounds like nucleic acids (anti-GMP(bio), anti-GMP(ups), and anti-DNA(hu)) (Figure 10b and Table 1). The two antibodies showing highest record for the three parameters (anti-cortisol and anti-dinitrophenol) suggest they are resistant molecules to degradation and/or the product of degradation of biomolecules by biotic and abiotic processes. Nucleic acids (e.g., anti-DNA (hu)), which also showed high record for the three parameters in the scatterplot (Figure 10b), might resist the degradation due to their association to minerals and the adoption of alternative structures under saline and/or low water content which are highly resistant to biological or chemical degradation [*Borin et al.*, 2008; *Sankaranarayanan et al.*, 2011].

[40] The distribution of antigen-antibody reactions along the lithological section shed some light on the origin of the most abundant antigens detected in AT2. Whereas anticortisol detection suggests the occurrence of triterpene and steroid-like lipids in bacteria and eukarya (see Figure S10 and Table 1), the prevalence of dinitrophenol in high

concentration in many of the samples suggests that it comes from the detection of phenol-bearing compounds resulting from the degradation of primary biomolecules [*Aiken et al*., 1985; *Stasiuk and Kozubek*, 2010; *Barakat et al*., 2012]. We have plotted (Figure 11a) the anti-dinitrophenol TRF against the total sum of antigens detecting nucleic acids (e.g., anti-DNA(hu), anti-cGMP(ups), and anti-cGMP(bio)) to infer the possible origin of the phenol-bearing compounds. Such a diagram shows data grouping in three different clusters: (1) samples showing negligible or absence of phenol-like compounds but some nucleic acids occurring in material samples in the upper part of the section, (2) samples showing low to medium (~10^3 to 10^4) anti-dinitrophenol TRF against high record of antigens of nucleic acids ($>5 \cdot 10^4$) in samples in the chloride-rich unit, and (3) samples with anti-dinitrophenol TRF ranging from ~0 to $2 \cdot 10^4$ but TRF of nucleic acids lower than $2 \cdot 10^4$ in samples occurring in the nitrate- and perchlorate-rich unit. When rating the anti-dinitrophenol against the nucleic acid TRF in the lithostratigraphic section (Figure 11b), we obtain the three different zones as the following: an upper detrital with no phenol-bearing compounds but has lower nucleic acids, an intermediate chloride-rich unit with high concentration of nucleic acids, and a lower nitrate- and perchlorate-rich unit with higher concentration in phenol-bearing compounds but depleted in nucleic acids.

[41] Such a distribution maybe a consequence of the differential preservation and age of the materials that trapped the biomolecules. The upper deposits that correspond to recent detrital compounds of an alluvial fan were formed under less saline ephemeral conditions that likely favored the preservation of microbial biomolecules like nucleic acids but not the formation of phenol-bearing substances, which require time for degradation of lipidic compounds. The intermediate and chloride-rich materials (samples AT2-4d2, AT2-4e1, and AT2-4e2) showing very low relative amount of anti-dinitrophenol/anti-nucleic acids suggest a very high preservation potential for samples older than 2–5 Ma. In the lower nitrate- and perchlorate-rich materials, the phenol-bearing compounds are much more abundant (Figures 11a and 11b), whereas the nucleic acids show a decrease in concentration. Such an increase in phenolic compounds suggests a higher degradation of samples formed some millions of years before under highly saline and oxidizing conditions [*Chong et al*., 2007] as prevailing for the formation of nitrates like nitranite and the perchlorate minerals, which are much older than the chlorite-rich deposits of La Soledad Formation [*Chong-Díaz et al*., 1999; *Sáez et al*., 1999]. Indeed, phenol-bearing molecules can be the result of the active degradation of phenolic compounds found in algae [*Barakat et al*., 2012]. However, the presence of nucleic acids in the nitrate- and perchlorate-rich deposits (Figures 10 and 11) also suggests that they can preserve biomolecules bearing high biological information.

[42] Besides physicochemical conditions, age is also an essential parameter controlling the preservation degree of the biological information recorded in sedimentary materials. The saline units sampled in the subsurface correspond to two different sedimentary units within the Soledad Formation as follows: (1) the upper halite-rich unit with an age between 2 and 5 Ma [*Chong-Díaz et al*., 1999; *Sáez et al*., 1999], and (2) a lower perchlorate-bearing unit with an age ranging from 5 to 30 Ma [*Chong et al*., 2007]. Consequently, these salts have a preservation potential that can provide biological information about the organisms that inhabited the salty bodies of water over tens of millions of years. It is possible that, assuming no exposure of saline rocks to persistent high water activity conditions, salt-rich deposits could maintain an exceptional biological record over millions of years [*Park et al*., 2009].

6. Conclusions

[43] The application of different complimentary techniques ranging from geological reconnaissance and geophysical sounding to molecular analysis has enabled a detailed characterization of biomolecular preservation in saline deposits of the Atacama Desert. After a geological survey of the Salar Grande, one site, marginal to the main lacustrine body of the Salar Grande, was selected to meet physical, petrologic, mineral, and geochemical requirements including the presence of both chloride- and perchlorate-rich salts. Resistivity surveys of these sites suggested that the saline deposits were affected by recent hydrological activity at depths greater than 6 m. By combining both geological survey and geophysical sounding, we selected site AT2 to drill for samples that were not affected by subsurface water flow in recent times. Petrological, mineralogical, and geochemical analyses of the subsurface deposits enabled us to identify three different sedimentary units including an uppermost detrital unit, an intermediate chloride-rich unit, and a lower unit enriched with nitrates and perchlorates. Although some work on the soils of the Atacama Desert has indicated that they have a poor or negligible preservation potential [*Navarro-González et al*., 2003], the organic and molecular analysis of the subsurface saline samples presented here indicates that under some circumstances they may host intact biomolecules. The analytical results demonstrate that the salty deposits sampled in the subsurface at AT2 have preserved microbial remains in the form of various organic compounds and biomolecules. Additionally, preservation in the perchlorate-rich unit, formed under oxidizing conditions and very low water activity, is sufficiently high to yield biological information in great detail through an excellent biomolecular record [*Parro et al*., 2011b]. This study also demonstrates that detailed stratigraphic and geochemical analyses conducted in conjunction with molecular analysis identified specific horizons within a salt deposit to focus on for looking for biomolecules, a very valuable tool when using a rover.

[44] Based on the molecular results from the salt units of Atacama, it is clear that salt mineral matrices may be excellent for preserving molecular information over millions of years [*Park et al*., 2009]. This is due to diagenesis driven by a fast dehydration process such as that which occurred in the Salar Grande sedimentary units, when surface and subsurface water is removed in the hyperarid saline basin over a few thousand years by different geological processes [*Sáez et al*., 1999]. Under these conditions, microbial activity and physical and chemical processes should have accordingly ceased, thus inhibiting the degradation of biomolecules.

[45] However, an exceptional molecular record does not necessarily mean viable cells [*McGenity et al*., 2000]. Key biomolecules including DNA and RNA rapidly degrade in

the absence of cellular metabolic processes, as damage from radiation, oxidation, and other deleterious processes cannot be repaired [*Willerslev and Hebsgaard*, 2005]. The rate of destruction is also dependent upon the temperature and salinity, both of which inhibit the activity of nucleases and the rate of reactions that hydrolyze and cleave the bonds in nucleic acids [*Willerslev and Cooper*, 2005]. Nevertheless, it has been observed that preservation of DNA is possible within the deep geological record of the Earth. Although it is still controversial, *Park et al*. [2009] reported the extraction of DNA from 419 Ma Silurian salts that likely derive from the genome of unclassified groups of ancient haloarchaea. Interestingly, those Silurian salty materials correspond to unaltered halite-rich sediments where the water activity should be around 0.75 or lower [*Satterfield et al*., 2005]. Therefore, preservation of biological information in chloride-rich and perchlorate materials over geologic timescales is plausible under suitable physicochemical conditions including consistently low water activity and temperature.

[46] **Acknowledgments.** We thank the Associate Editor and two anonymous reviewers, whose suggestions have strongly improved the paper. This research is being supported by the *Subdirección General de Proyectos de Investigación* of the Spanish *Ministerio de Ciencia e Innovación* (MICINN) grants AYA 2009-11681, AYA2008-04013, and AYA2011-24803.

References

Aiken, G. R., D. M. McKnight, R. L. Warsaw, and P. MacCarthy (1985), An introduction to humic substances in soil, sediment and water, in *Humic Substances in Soil Sediment and Water*, edited by G. R. Aiken, D. M. McKnight, R. L. Warsaw, and P. MacCarthy, pp. 1–9, Wiley, New York.

Barakat, A. O., S. Baumgart, P. Brocks, B. M. Scholz-Böttcher, and J. Rullkötter (2012), Alkylated phenol series in lacustrine black shales from the Nördlinger Ries, southern Germany, *J. Mass Spectrom.*, *47*, 987–994.

Blanco, Y., L. A. Rivas, M. Ruiz-Bermejo, and V. Parro (2012), Detection of mellitic acid in the surface and subsurface of the Atacama Desert terrestrial analog, *EPSC Abstracts*, 7, EPSC2012-83.

Borin, S., E. Crotti, F. Mapelli, I. Tamagnini, C. Corselli, and D. Daffonchio (2008), DNA is preserved and maintains transforming potential after contact with brines of the deep anoxic hypersaline lakes of the Eastern Mediterranean Sea, *Saline Sys.*, *4*, doi:10.1186/1746-1448-4-10.

Catling, D. C., M. W. Claire, K. J. Zahnle, R. C. Quinn, B. C. Clark, M. H. Hecht, and S. Kounaves (2010), Atmospheric origins of perchlorate on Mars and in the Atacama, *J. Geophys. Res.*, *115*, E00E11, doi:10.1029/2009JE003425.

Chin, K.-J., and P. H. Janssen (2002), Propionate formation by *Opitutus terrae* in pure culture and in mixed culture with a hydrogenotrophic methanogen and implications for carbon fluxes in anoxic rice paddy soil, *Appl. Environ. Microbiol.*, *68*, 2089–2092.

Chong, G., A. J. Gajardo Cubillos, A. J. Hartley, and T. Moreno (2007), Industrial minerals and rocks, in *The Geology of Chile*, edited by T. Moreno, and W. Gibbons, pp. 201–214, The Geological Society of London, London.

Chong-Díaz, G., M. Mendoza, J. García-Veigas, J. J. Pueyo, and P. Turner (1999), Evolution and geochemical signatures in a Neogene forearc evaporitic basin: The Salar Grande (Central Andes of Chile), *Palaeogeogr. Palaeoclimatol. Palaeoecol.*, *151*, 39–54.

Clark, B. C., R. V. Morris, S. M. McLennan, R. Gellert, B. Jolliff, A. H. Knoll, S. W. Squyres, T. K. Lowenstein, D. W. Ming, and N. J. Tosca (2005), Chemistry and mineralogy of outcrops at Meridiani Planum, *Earth Planet. Sci. Lett.*, *240*, 73–94.

Davila, A. F., B. Gómez-Silva, A. de los Rios, C. Ascaso, H. Olivares, C. P. McKay, and J. Wierzchos (2008), Facilitation of endolithic microbial survival in the hyperarid core of the Atacama Desert by mineral deliquescence, *J. Geophys. Res.*, *113*, G01028, doi:10.1029/2007JG000561.

Dunai, T. J., G. A. González López, and J. Juez-Larré (2005), Oligocene–Miocene age of aridity in the Atacama Desert revealed by exposure dating of erosion-sensitive landforms, *Geology*, *33*, 321–324.

Dutton, M. V., and C. S. Evans (1996), Oxalate production by fungi: Its role in pathogenicity and ecology in the soil environment, *Can. J. Microbiol.*, *42*, 881–895.

Eglinton, G., and G. A. Logan (1991), Molecular preservation, *Philos. Trans. R. Soc. Lond. B Biol. Sci.*, *333*, 315–328.

Fazio, S. A., D. J. Uhlinger, J. H. Parker, and D. C. White (1982), Estimations of uronic acids as quantitative measures of extracellular and cell wall polysaccharide polymers from environmental samples, *Appl. Environmental Microbiol.*, *43*, 1151–9.

Fernández-Remolar, D. C., O. Prieto-Ballesteros, N. Rodríguez, F. Gómez, R. Amils, J. Gómez-Elvira, and C. R. Stoker (2008), Underground habitats in the Río Tinto Basin: A model for subsurface life habitats on Mars, *Astrobiology*, *8*, 1023–1047.

Fish, S. A., T. J. Shepherd, T. J. McGenity, and W. D. Grant (2002), Recovery of 16S ribosomal RNA gene fragments from ancient halite, *Nature*, *417*, 432–436.

Glotch, T. D., J. L. Bandfield, L. L. Tornabene, H. B. Jensen, and F. P. Seelos (2010), Distribution and formation of chlorides and phyllosilicates in Terra Sirenum, Mars, *Geophys. Res. Lett.*, *37*, L16202, doi:10.1029/2010GL044557.

Gramain, A., G. Chong Díaz, C Demergasso, Tk. Lowenstein, Tj. Mcgenity, (2011), Archaeal diversity along a subterranean salt core from the Salar Grande (Chile)., *Environmental Microbiology*, *13*, 2105–2121.

Griffith, J. D., S. Willcox, D. W. Powers, R. Nelson, and B. K. Baxter (2008), Discovery of abundant cellulose microfibers encased in 250 Ma Permian halite: A macromolecular target in the search for life on other planets, *Astrobiology*, *8*, 215–228.

Hammer, Ø., D. A. T. Harper, and P. D. Ryan (2001), PAST: Palaeontological Statistics software package for education and data analysis, *Palaeontol. Electron.*, *4*, 9.

Hecht, M. H., et al. (2009), Detection of perchlorate and the soluble chemistry of Martian soil at the Phoenix Lander Site, *Science*, *325*, 64–67, doi:10.1126/science.1172466.

Houtkooper, J. M., and D. Schulze-Makuch (2010), Xerophiles on Mars: Possible evolutionary strategies using hydrogen peroxide and perchlorates, *Proceedings of the Astrobiology Science Conference* 2010, paper 5382.

Jackson, W. A., T. Anderson, G. Harvey, G. Orris, S. Rajagopalan, and N. Kang (2006), Occurrence and formation of non-anthropogenic perchlorate, in *Perchlorate: Environmental Occurrence, Interactions and Treatment*, edited by B. Gu, and J. D. Coates, pp. 49–69, Springer, US.

Kim, S., L. A. Kaplan, and P. G. Hatcher (2006), Biodegradable dissolved organic matter in a temperate and a tropical stream determined from ultra-high resolution mass spectrometry, *Limnol. Oceanogr.*, *51*, 1054–1063.

King, P. L., D. T. Lescinsky, and H. W. Nesbitt (2004), The composition and evolution of primordial solutions on Mars, with application to other planetary bodies, *Geochim. Cosmochim. Acta*, *68*, 4993–5008.

Lester, E. D., M. Satomi, and A. Ponce (2007), Microflora of extreme arid Atacama Desert soil, *Soil Biol. Biogeochem.*, *39*, 704–708.

Loke, M. H., and R. D. Barker (1996), Rapid least-squares inversion of apparent resistivity pseudosections by a quasi-Newton method, *Geophys. Prospect.*, *44*, 131–152.

Lowenstein, T. K., J. Li, C. Brown, S. M. Roberts, T.-L. Ku, S. Luo, and W. Yang (1999), 200 k.y. paleoclimate record from Death Valley salt core, *Geology*, *27*, 3–6.

McGenity, T. J., R. T. Gemmell, W. D. Grant, and H. Stan-Lotter (2000), Origins of halophilic microorganisms in ancient salt deposits, *Environ. Microbiol.*, *2*, 243–250.

McLennan, S. M., J. F. Bell III, W. M. Calvin, P. R. Christensen, B. C. Clark, P. A. de Souza, J. Farmer, W. H. Farrand, D. A. Fike, and R. Gellert (2005), Provenance and diagenesis of the evaporite-bearing Burns formation, Meridiani Planum, Mars, *Earth Planet. Sci. Lett.*, *240*, 95–121.

Michalski, G., J. K. Böhlke, and M. Thiemens (2004), Long term atmospheric deposition as the source of nitrate and other salts in the Atacama Desert, Chile: New evidence from mass-independent oxygen isotopic compositions, *Geochim. Cosmochim. Acta*, *68*, 4023–4038.

Murchie, S. L., et al. (2009), A synthesis of Martian aqueous mineralogy after one Mars year of observations from the Mars Reconnaissance Orbiter, *J. Geophys. Res.*, *114*, E00D06, doi:10.1029/2009JE003342.

Navarro-González, R., E. Vargas, J. de la Rosa, A. C. Raga, and C. P. McKay (2010), Reanalysis of the Viking results suggests perchlorate and organics at midlatitudes on Mars, *J. Geophys. Res.*, *115*, E12010, doi:10.1029/2011JE003854.

Navarro-González, R., et al. (2003), Mars-like soils in the Atacama Desert, Chile, and the dry limit of microbial life, *Science*, *302*, 1018–1021.

Osterloo, M. M., V. E. Hamilton, J. L. Bandfield, T. D. Glotch, A. M. Baldridge, P. R. Christensen, L. L. Tornabene, and F. S. Anderson (2008), Chloride-bearing materials in the southern highlands of Mars, *Science*, *319*, 1651–1654.

Park, J. S., R. H. Vreeland, B. C. Cho, T. K. Lowenstein, M. N. Timofeeff, and W. D. Rosenzweig (2009), Haloarchaeal diversity in 23, 121 and 419 MYA salts, *Geobiology*, *7*, 515–523.

Parro, V., et al. (2008), SOLID2: An antibody array-based life-detector instrument in a Mars Drilling Simulation Experiment (MARTE), *Astrobiology*, *8*, 987–999.

Parro, V., et al. (2011a), Classification of modern and old Río Tinto sedimentary deposits through the biomolecular record using a life marker biochip: Implications for detecting life on Mars, *Astrobiology*, *11*, 29–44.

Parro, V., et al. (2011b), A microbial oasis in the hypersaline Atacama subsurface discovered by a life detector chip: Implications for the search of life on Mars, *Astrobiology*, *11*, 969–996.

Pueyo, J. J., G. Chong, and A. Jensen (2001), Neogene evaporites in desert volcanic environments: Atacama Desert, northern Chile, *Sedimentol.*, *48*, 1411–1431.

Reijs, J., and K. McClay (1998), Salar Grande pull-apart basin, Atacama Fault System, northern Chile., *Geological Society*, London, Special Publications, *135*, 127–141.

Risacher, F., and B. Fritz (2009), Origin of salts and brine evolution of Bolivian and Chilean Salars, *Aquat. Geochem.*, *15*, 123–157.

Rivas, L. A., M. García-Villadangos, M. Moreno-Paz, P. Cruz-Gil, J. GóMez-Elvira, V. C. Parro, (2008), A 200-antibody microarray biochip for environmental monitoring: Searching for universal microbial biomarkers through immunoprofiling, *Analytical Chemistry*, *80*, 7970–7979.

Santos, H., and M. S. da Costa (2002), Compatible solutes of organisms that live in hot saline environments, *Environ. Microbiol.*, *4*, 501–9.

Sáez, A., L. Cabrera, A. Jensen, and G. Chong (1999), Late Neogene lacustrine record and palaeogeography in the Quillagua-Llamara basin, Central Andean fore-arc (northern Chile), *Palaeogeogr. Palaeoclimatol. Palaeoecol.*, *151*, 5–37.

Schmitt-Kopplin, P., et al. (2012), Dissolved organic matter in sea spray: A transfer study from marine surface water to aerosols., *Biogeosci.*, *9*, 1571–1582.

Sankaranarayanan, K., M. N. Timofeeff, R. Spathis, T. K. Lowenstein, and J. K. Lum (2011), Ancient microbes from halite fluid inclusions: Optimized surface sterilization and DNA extraction, *PLoS One*, *6*, e20683, doi:10.1371/journal.pone.0020683.

Satterfield, C. L., T. K. Lowenstein, R. H. Vreeland, and W. D. Rosenzweig (2005), Paleobrine temperatures, chemistries, and paleoenvironments of Silurian Salina Formation F-1 Salt, Michigan Basin, U.S.A., from petrography and fluid inclusions in halite, *J. Sediment. Res.*, *75*, 534–546.

Schmidt, F., M. Elvert, B. P. Koch, M. Witt, and K.-U. Hinrichs (2009), Molecular characterization of dissolved organic matter in pore water of continental shelf sediments, *Geochim. Cosmochim. Acta*, *73*, 3337–3358.

Schmitt-Kopplin, P., A. Gelencsér, E. Dabek-Zlotorzynska, G. Kiss, N. Hertkorn, M. Harir, Y. Hong, and I. Gebefügi (2010), Analysis of the unresolved organic fraction in atmospheric aerosols with ultrahigh-resolution mass spectrometry and nuclear magnetic resonance spectroscopy: Organosulfates as photochemical smog constituents, *Anal. Chem.*, *82*, 8017–8026.

Simpson, E. H. (1949), Measurement of diversity, *Nature*, *163*, 688.

Spiro, B., and G. Chong Díaz (1996), Origin of the sulfate in the Salar de Atacama and the Cordillera de la Sal, initial results of an isotopic study, *Third International Symposium on Andean Geodynamics*, pp. 703–705, St Malo, France.

Stan-Lotter, H., S. Leuko, A. Legat, and S. Fendrihan (2006), The assessment of the viability of halophilic microorganisms in natural communities, in *Methods in Microbiology: Extremophiles*, edited by A. Oren, and F. Rainey, pp. 569–584, Elsevier, Oxford, U. K.

Stasiuk, M., and A. Kozubek (2010), Biological activity of phenolic lipids, *Cell. Mol. Life Sci.*, *67*, 841–860.

Tosca, N. J., A. H. Knoll, and S. M. McLennan (2008), Water activity and the challenge for life on early Mars, *Science*, *320*, 1204–1207.

Trumpolt, C. W., M. Crain, G. D. Cullison, S. J. P. Flanagan, L. Siegel, and S. Lathrop (2005), Perchlorate: Sources, uses, and occurrences in the environment, *Rem. J.*, *16*, 65–89.

Wierzchos, J., B. Cámara, A. De Los Ríos, A. F. Davila, I. M. Sánchez Almazo, O. Artieda, K. Wierzchos, B. Gómez-Silva, C. P. McKay, and C. Ascaso (2011), Microbial colonization of Ca-sulfate crusts in the hyperarid core of the Atacama Desert: Implications for the search for life on Mars, *Geobiology*, *9*, 44–60.

Willerslev, E., and A. Cooper (2005), Review paper. Ancient DNA, *Proc. R. Soc. B: Biol. Sci.*, *272*, 3–16.

Willerslev, E., and M. B. Hebsgaard (2005), New evidence for 250 Ma age of halotolerant bacterium from a Permian salt crystal: Comment and reply, *Geology*, *33*, e93–e93.